

Full Paper

Magnetically Assembled Multisegmented Nanowires and Their Applications

Mangesh A. Bangar,^a Carlos M. Hangarter,^a Bongyoung Yoo,^b Youngwoo Rheem,^a Wilfred Chen,^a Ashok Mulchandani,^{a*} Nosang V. Myung^{a*}

^a Department of Chemical and Environmental Engineering and Center for Nanoscale Science and Engineering, University of California-Riverside, Riverside, CA 92521, USA

^b Division of Materials and Chemical Engineering, Hanyang University, Ansan 426-791, Korea

*e-mail: adani@engr.ucr.edu; myung@engr.ucr.edu

Received: July 31, 2008

Accepted: September 26, 2008

Abstract

Here we report a cost effective and versatile way of synthesizing and assembling multi-functional (e.g., gold-polypyrrole-nickel-gold) nanowires. Multisegmented nanowires were synthesized using electrodeposition method for precise control over segment dimensions for proper expression of material functionality. The nanowires were integrated on microfabricated electrodes using magnetic dipole interactions between the ferromagnetic segment in the nanowire and the ferromagnetic electrodes. The electrical properties of multisegmented nanowires showed semiconducting behavior with the activation energy of ca. 0.27 eV for the conducting polymer segment of the nanowire. These nanowire devices showed response towards light and exposure to ammonia, demonstrating their potential use as photonic device and gas sensor, respectively.

Keywords: Anodized alumina, Electrodeposition, Nanowires, Polypyrrole, Photonic devices, Ammonia, Gas sensor

DOI: 10.1002/elan.200804372

1. Introduction

Conducting polymers are emerging materials for electronic devices, exhibiting properties from metals to insulators as their electrical properties can be reversibly modulated by controlling the dopant type and level [1–3]. This class of polymers also show semiconductor-like properties such as band-gap/activation energy and photoconductivity. These tunable properties along with scalability and ease of processing make them economically viable for practical use. In particular, a variety of conducting polymers have shown promise as low-power sensor materials tailored to detect a wide range of chemical compounds [4–6]. Moreover, their benign synthesis conditions allow for concomitant biomolecule entrapment during polymerization, leading to single-step biofunctionalized conducting polymers [7–10]. Recently, some efforts have also been geared towards the use of conducting polymer nanowires/nanotubes for photoelectric sensors [11, 12].

While conventional conducting polymer based sensors are fabricated by thin film techniques [13, 14], one-dimensional nanostructures such as nanowires and nanotubes are very attractive for sensing applications because their small dimensions and high aspect ratios are ideal for high density multiplexed sensing systems [9, 15, 16]. Despite several examples of conducting polymer nanowire/nanotube based devices assembled using techniques such as dip-pen nanolithography [17, 18], microcontact printing [19], electro-

spinning [20–22], mechanical stretching [23], in situ fabrication [7, 24, 25], lithographic techniques [26–27] and random dispersion of nanowires on top of prefabricated electrodes [16, 28, 29], the inability to manipulate and address these nanostructures in a rational manner has limited their potential with low yield and high cost. In order to realize conducting polymer based nanodevices, cost-effective, manufacturable fabrication and assembly techniques are required.

In this study, we have utilized a novel approach to assemble conducting polymer nanostructures on prefabricated electrodes by synthesizing multisegmented nanowires with two functional midsections, the conducting polymer (i.e., polypyrrole) and a nickel segment, for sensing and assembling, respectively. Polypyrrole (Ppy) has demonstrated excellent sensitivity towards gas molecules such as ammonia, hydrogen sulfide, and carbon dioxide [30] and nickel's inherent ferromagnetism provides a mean for nanowire manipulation. Nanowire fabrication exercised only template directed electrodeposition, allowing further functionality with gold terminating segments for good electrical contact. The directionality of nanowires was controlled by an external magnetic field while ferromagnetic electrodes were essential for controlled placement of nanowires. Devices fabricated in this fashion were characterized with temperature dependent electrical transport measurements and investigated for their photocurrent response toward light and chemiresistive response towards ammonia gas.

2. Experimental

2.1. Multisegmented Nanowire Synthesis

Multisegmented nanowires were synthesized in alumina templates (Whatman Anodisc 200 nm pore diameter), which served as a scaffold for electrodeposition. The schematic of fabrication steps is illustrated in Figure 1A. Initially, one side of the template was sputter coated with gold (Au) using an Emitech K550 desktop sputter machine, which served as the seed layer for electrodeposition. A three-electrode configuration was used to deposit nanowires. A platinum coated metal strip and saturated calomel electrode (SCE) were used as counter and reference electrode, respectively. All materials were electrodeposited using a multichannel EG&G PAR VMP2 potentio/galvanostat in the chronopotentiometric mode (constant current/current-density mode). Gold segments were electrodeposited from a commercial gold electroplating solution (Technic-Gold 25 ES) at 60 °C. Ppy segments were electrodeposited from an aqueous solution of 0.5 M pyrrole monomer (99.9% purity and distilled prior to use) in 0.2 M LiClO₄ solution. Nickel segment was electrodeposited from an electrolyte that consisted of 0.91 M Ni(H₂NSO₃)₂ + 0.10 M H₃BO₃ + 30 ppm HCl. The template was thoroughly

rinsed with deionized water after deposition of each segment. The length of each segment was controlled by controlling the time of deposition. After electrodeposition, the Au seed layer was mechanically removed, followed by washing of the alumina template with acetone to remove any residues from earlier steps. The template was then dissolved in 5 M NaOH. Suspended nanowires were collected from NaOH by centrifugation, washed with nanopure water followed by resuspension in isopropanol. The details of Ppy and Nickel segment deposition under different electrodeposition conditions are discussed in Section 3.1.

2.2. Magnetic Trapping and Alignment of Multisegmented Nanowires

Silicon substrates with predefined electrodes were used for magnetic alignment of nanowires. At least one of the electrodes in the pair was electrodeposited with a ferromagnetic material (i.e., nickel or cobalt) followed by a thin layer of gold to prevent the oxidation of the electrode surface. The silicon substrate was then placed between two external bar magnets with a magnetic field of 1.26 kilo-gauss and 5 μ L of the nanowire suspension was manually pipetted over the electrodes. Magnetically aligned and electrically

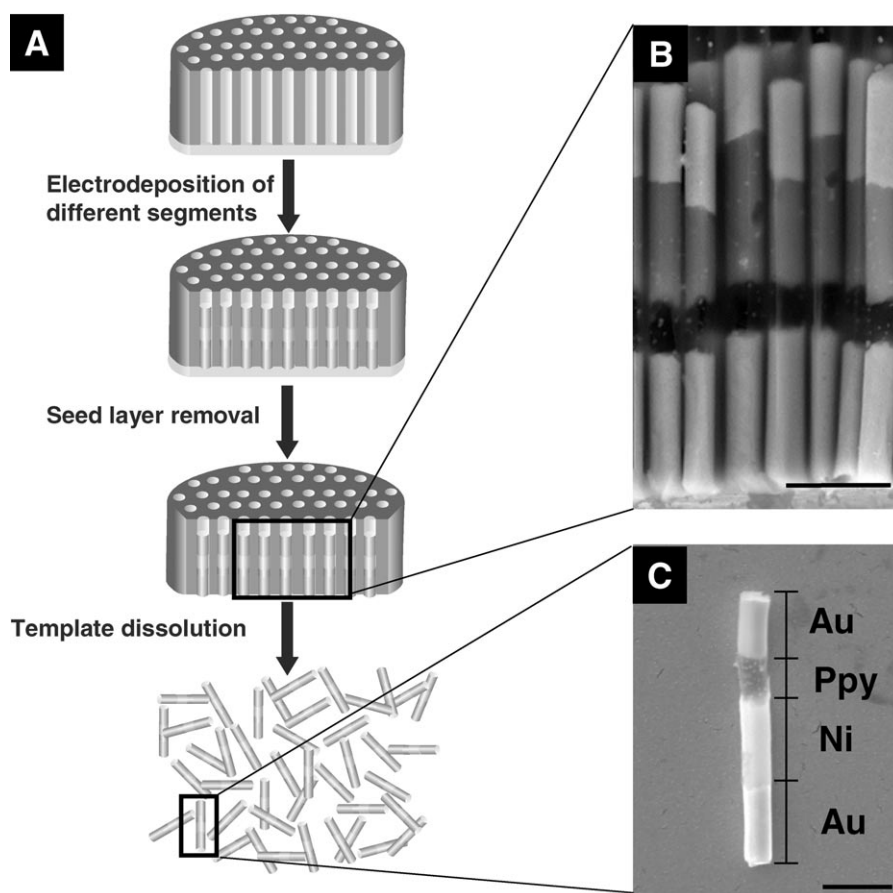


Fig. 1. A) Schematic of different steps involved in synthesis and suspension of multisegmented nanowires. B) Cross-sectional SEM image of four segment nanowires inside the alumina template. C) SEM image of single suspended nanowire showing different segments of the nanowire. (Scale bar = 1 μ m).

contacted multisegmented nanowire devices were obtained after the solvent evaporated. For simple/random alignment (without spatial control) of these nanowires, the nanowire suspension was dropped on the microfabricated gold electrodes under the influence of external magnetic field. After magnetic alignment of the nanowires, the substrate was examined using a digital optical microscope (Hirox KH-3000). Further high resolution visual characterization was done using a scanning electron microscope (Phillips XL30-FEG).

2.3. Electrical, Optoelectronic, and Sensing Measurements

Operational nanowire devices were wire bonded on to larger circuits for further characterization with a West Bond Model No. 7443A. All the electrical measurements were carried out using a semiconductor parameter analyzer (HP 4155A). Low temperature current–voltage (I – V) measurements were performed with a physical property measurement system (Quantum Design PPMS). Optoelectronic responses of single nanowire devices were characterized using white light and a 75 Watt xenon lamp irradiated at 550 nm attached to a PTI model A1010 monochromator. For NH_3 sensing experiments, analyte gas along with the carrier gas was passed over the sensor at a combined flow rate of 150 standard cubic centimeters per minute (sccm) using Alicat Scientific Inc. mass flow controllers. The device was enclosed in a glass chamber and sealed in a dark furnace as the sensing response was recorded using a chemiresistive (two-point contact) sensor configuration [31, 32].

3. Results and Discussion

3.1. Synthesis and Assembly of Multisegmented Nanowires

Multisegmented gold-polypyrrole (Ppy)-nickel-gold nanowires were electrochemically fabricated using alumina template (Fig. 1). The most essential factor for assembling nanowires on prefabricated electrodes is precise control over the length and uniformity of each segment in the nanowire. In the present study, such control was established using an all-electrochemical approach with galvanostatic deposition, adjusting nanowire length with deposition time/charge. For device functionality it is crucial that the segment of interest (Ppy) lie between the electrodes upon assembly. However, for magnetic alignment the nickel segment must also be positioned in the midsection, as these ferromagnetic nanowires have been shown to align adjacent to ferromagnetic electrodes. This configuration requires that the nickel segment be sufficiently long for nanowire manipulation but smaller than the electrode gap to prevent bypassing the Ppy by shorting through the nickel. Moreover, the functional material (Ppy) and the ferromagnetic nickel segment do not form good electrical contact as the Ppy surface may degrade

and the nickel is prone to oxide formation. Thus the final segmented nanowires of Au-Ppy-Ni-Au were fabricated with gold segments for electrical contact and a Ppy-Ni midsection for sensing and magnetic alignment, respectively.

At low current density (e.g., 1 to 2 mA cm⁻²), the gold electrolyte solution showed 100% current efficiency and precise control over the length of the 1st and 4th Au segments was achieved. Ppy deposition however did not show the linear correlation between the time of deposition and the length of the Ppy segment (Fig. 2). Ppy electrodeposition was carried out at two different current densities of 2 and 5 mA/cm². The Ppy electrodeposition showed linear correlation between the time of deposition and the length of Ppy segment deposited only for short deposition times. However, for longer deposition periods the Ppy growth stagnated with no measurable increase in length indicating very poor deposition efficiency. The large disparities in saturation length with increasing current density, as can be seen from the Figure 2, may reside in the doping concentration or extended tubular formation. Although the nickel electrolyte used generally forms quality deposits for a range of current densities, i.e., 2 to 40 mA/cm², the deposition uniformity on top of Ppy was sensitive to the current density. At higher current densities (≥ 10 mA/cm²) nickel segments showed highly nonuniform and uncontrolled deposition. The higher deposition potentials at these current densities combined with the variances in the Ppy nanowire resistances and nucleation overpotentials promote rapid deposition in some pores while others undergo side reactions such as hydrogen gas evolution. This leads to trapping of hydrogen gas bubbles in some of the alumina pores with very poor/no deposition and a reduced effective area, producing exaggerated nickel segments in the other pores and nonuniformity. This nonuniformity can be avoided if nickel nucleation can be achieved on all Ppy nanowire ends. Thus a forced nucleation step on top of Ppy segments was adopted for the nickel segment, which will be referred to as 'striking' in further text. During striking a very high current density (250 mA/cm²) was applied for one second. This forced nucleation step exhausts the nickel ions from the pores of the alumina template requiring a relaxation time of about 2 minutes before the nickel ion concentration is replenished within the pores and electrodeposition at the normal current density can proceed. From Figure 3 it can be seen that the striking improved the uniformity of nickel segments deposited on top of shorter (0.5 microns in long) Ppy segments, with more pronounced improvements in uniformity at high current densities. The striking, however, was not sufficient in curtailing this nonuniformity for longer Ppy segments (data not shown). As a result, and for reduced resistance, the length of the Ppy segment was kept shorter (≤ 0.5 μm), with optimized lengths depicted in Figure 1B and C.

The addition of the ferromagnetic nickel segment, which can be magnetized in presence of an external magnetic field, allows these nanowires to act like tiny magnets that not only interact with an external magnetic field but also interact with one another and ferromagnetic electrodes. The im-

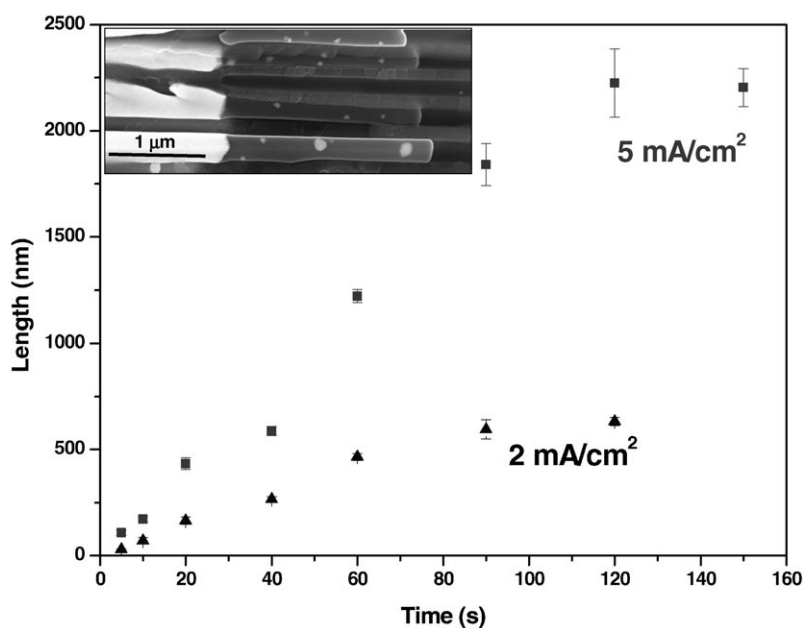


Fig. 2. Length of Ppy segment deposited as function of deposition time at different current densities. Inset shows an SEM image of Ppy segment deposited on Au (at 5 mA/cm², the length of Ppy ca. 2 µm) segment inside the alumina template.

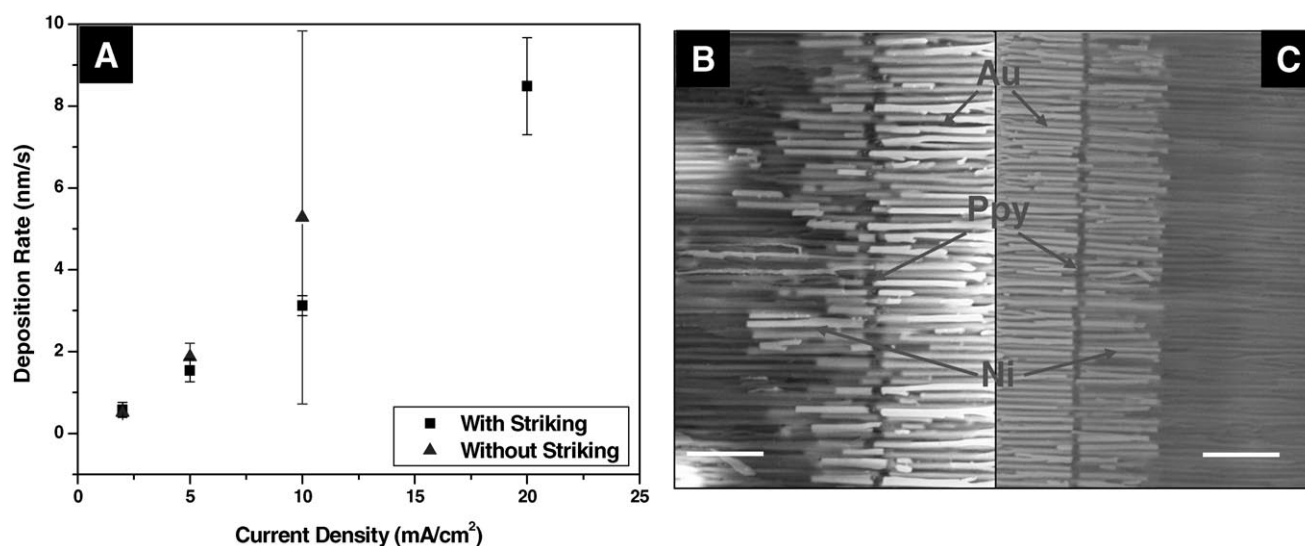


Fig. 3. Left: A) Deposition rate of Ni segment on top of 0.4 µm Ppy segment as a function of current density applied with (squares) and without (triangles) striking. Right: SEM images showing the deposition profile for Ni without (B) and with (C) striking at 20 mA/cm². (Scale bar = 3 µm)

posed magnetic field aligns the nanowires in solution parallel to the magnetic field due to the substantially stronger shape anisotropy of the nickel segment, magnetizing the nickel along its cylindrical axis or magnetic easy axis, proving to be an efficient material for magnetic alignment [33]. As shown in Figure 4A, in the presence of an external magnetic field, the ferromagnetic electrodes magnetize and behave as micromagnets, creating strong local fields at the edge of the electrodes where magnetic poles are formed. These localized magnetic fields dominate nanowire-nanowire dipole interactions for preferential

nanowire alignment adjacent to the ferromagnetic electrode. Although, electrode pairs with a single ferromagnetic electrode (the other is gold) did not always facilitate bridging of both the Ni and Ppy segment, matching pairs of ferromagnetic electrodes dramatically improved yield. These observations were attributed to both the difference in magnetic fields and the magnetic properties of the Ni segment's neighboring materials. For a single ferromagnetic electrode the magnetic field is strongest at a single edge allowing it to extend further with either end of the Ni segment next to the electrode. However for two ferromag-

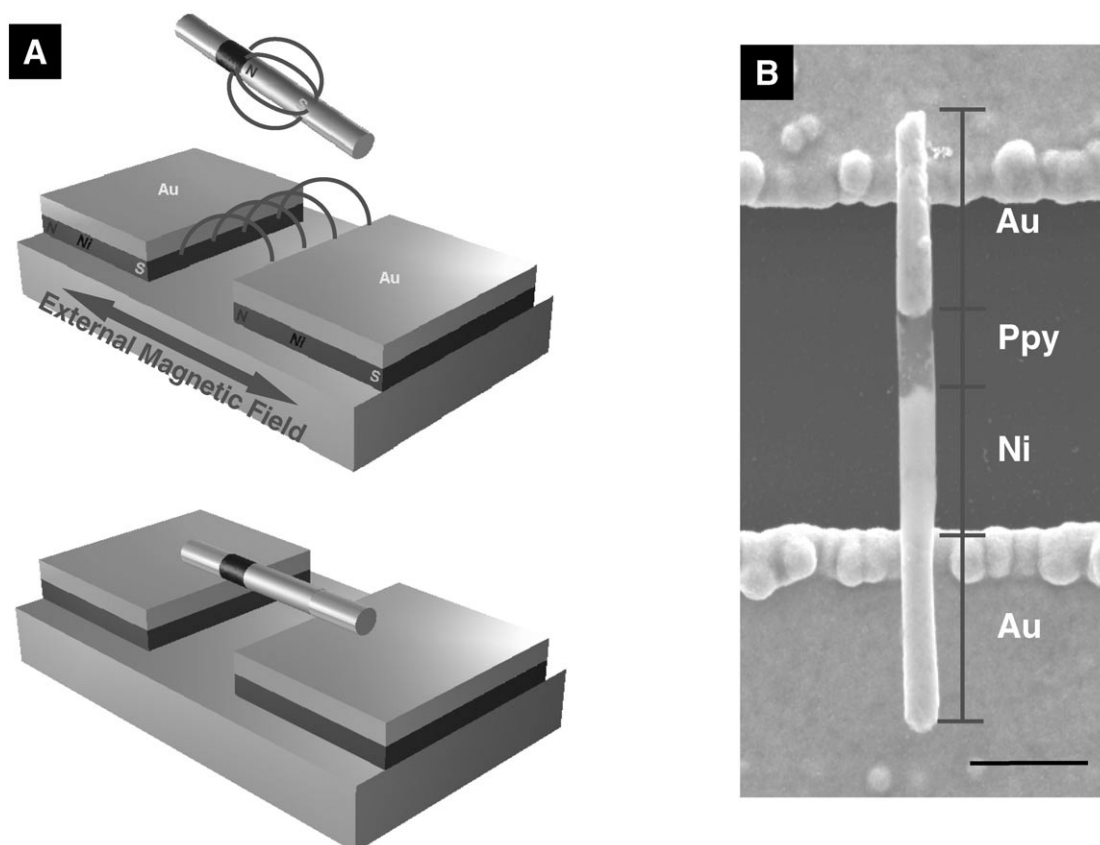


Fig. 4. A) Schematic illustration of the magnetic assembly of multisegmented nanowires. The lines represent the magnetic field of the nanowire and the ferromagnetic electrodes. Bottom figure showing the placement of different segments of the nanowire on the contact electrodes. B) SEM image of single nanowire device assembled using magnetic assembly on prefabricated electrodes. (Scale bar = 1 μm).

netic electrodes the magnetic field is focused between two edges and the paramagnetic Ppy segment will have a lower resistance in this gap than the diamagnetic gold segment. These magnetic interactions between the ferromagnetic electrodes and nanowire segments dictate the placement of the nanowires where the nickel segment is right next to one of the electrodes with the polypyrrole segment bridging the gap, and terminating gold segments overlapping the electrodes to provide better electrical contact. The resulting assemblage, Figure 4B, demonstrates precise control over alignment of multisegmented nanowires on prefabricated electrodes for single nanowire devices and suggests the potential for an array of high density nanowires with appropriately selected electrode geometry. In the absence of the ferromagnetic electrodes, these nanowires simply aligned in the direction of external magnetic field and were randomly positioned on the nonferromagnetic (Au) electrodes.

3.2. Electrical Characterization of Multisegmented Nanowires

Individual multisegmented nanowires displayed predominantly semiconducting characteristics with asymmetric s-

shaped $I-V$ curves and increased resistance at lower temperatures (data not shown) [16, 34–36]. The asymmetry in the $I-V$ curves has previously been assigned as the diode characteristics of these anisotropic one-dimensional structures [16]. The activation energy of these structures, calculated from the Arrhenius plot, is ca. 0.27 eV. The temperature coefficient of resistance (TCR), defined as:

$$TCR = (R/R_0 - 1)/(T - T_0) \quad (1)$$

was also determined for single multisegmented nanowires. Negative TCR values obtained and exponential decay confirms the semiconductor behavior for individual nanowires. The low conductivity values for these devices, ca. $10^{-3} - 10^{-4}$ S/cm were attributed to NaOH exposure during template dissolution, which is known to cause de-doping in Ppy samples with smaller molecular size dopants [28, 34, 35]. PPy reduction during Ni electrodeposition is another possible reason for the high resistance as the applied negative potential may also have caused brief egress of anionic perchlorate ions at the Ppy-Ni interface just prior to Ni deposition. This phenomenon may reduce a thin portion of the Ppy segment rendering it less conductive. A further investigation is, however, required for an accurate description.

3.3. Nanophotonic and Sensor Based on Single Multisegmented Nanowires

The Photoelectric response of these nanowire-based light sensors was studied using $I-V$ characterization in light and dark (data not shown). For light illumination, white light from the microscope objective was used. From the current values under dark (I_d) and light illuminated (I_{illum}) states at 0.5 V bias, a photocurrent ($I_{\text{ph}} = I_{\text{illum}} - I_d$) increase of about 10% was observed. When the $I-V$ curve was recorded with the light switched on and off, the graph followed, almost exactly, the $I-V$ curves under illuminated and dark states, respectively, within the temporal resolution of the data (data not shown). This indicates a very fast rise and decay time of the carriers (excitons) generated by photoexcitation. Photocurrent was strongly dependant on the field applied and varied linearly for lower fields of up to 1.3×10^3 V/cm. At higher fields, the increase in the photocurrent is nonlinear and has previously been suggested to be the effect of increased carrier mobility [37]. For precise control on the illumination wavelength and power, further characterization was done using a calibrated xenon lamp and a monochromator. Previous exposure of these single nanowire devices to light over a range of wavelengths indicated a maximum response (in terms of absolute value) in the visible spectrum at 550 nm (data not shown). Figure 5A shows a simple photocurrent on-off response of a single multisegmented nanowire at 0.5 V bias showing very reproducible photoresponse at an illumination intensity of $2 \mu\text{W}/\text{cm}^2$. The consistent response of the device indicates negligible or no thermal effects due to light illumination. The conductivity ratio of the device under the illumination conditions to that under dark is ca. 1.25.

Lastly, these nanowire based devices were studied for their response towards ammonia gas. NH_3 acts as a Lewis base, an electron is transferred to the polypyrrole backbone, reducing a single constituent rendering it electrically inactive thereby effectively reducing the mobility and conductivity due to its p-type semiconducting behavior [15, 28]. From Figure 5B it can be seen that the nanowire resistance increased upon exposure to ammonia. These devices showed a lower detection limit of about 75 ppm, and displayed a partially irreversible recovery, a characteristic quality for polypyrrole exposed to high concentrations of redox reactive analytes described previously [38]. The sensitivity of these structures was also relatively poor compared to alternative synthesis techniques such as electrospinning or chemical polymerization. Although dopant selection plays a role in sensitivity, the loss of sensitivity was primarily attributed to NaOH exposure during template dissolution as it has been shown to have significant effect on the optical [15, 39] and electrical [28] characteristics. The sensor sensitivity can be improved by dissolving the alumina templates in acidic media (i.e., phosphoric acid) instead of NaOH, which eliminates the overoxidation of polypyrrole.

Even though our work was limited to Ppy, other conducting polymers (e.g., polyaniline, polythiophene) can be integrated. The length of conducting polymer section needs

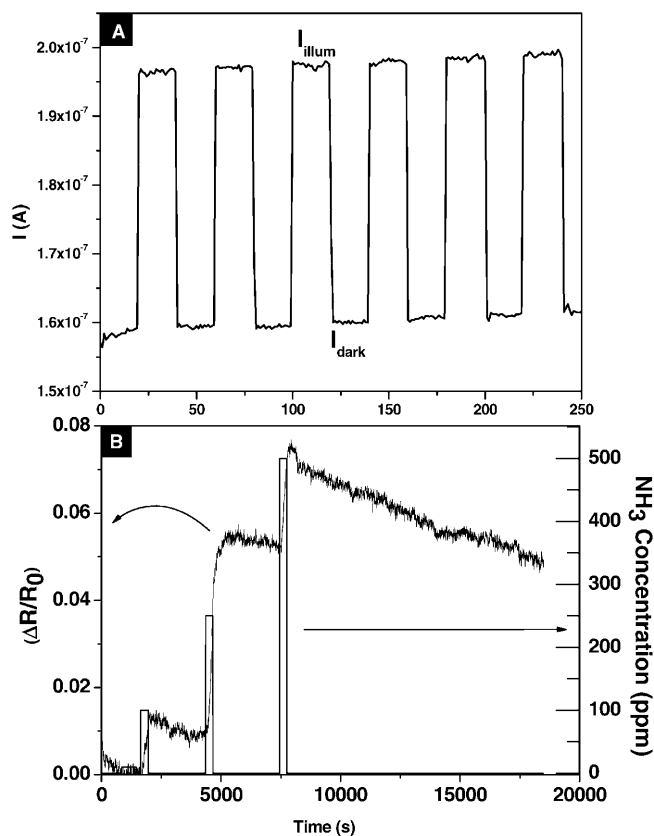


Fig. 5. A) Optoelectronic response of a multisegmented nanowire towards multiple exposure to light (550 nm) at 0.5 V bias. I_{illum} and I_{dark} correspond to current flowing through the nanowire under light illumination and under dark condition, respectively. B) The electrical response of single multisegmented nanowire upon exposure to different concentrations of ammonia at 0.5 V bias.

to be optimized for precise assembly and to control the overall resistance of the final device. Another factor to consider is the adhesion between conducting polymer and adjacent metal segment, which is crucial for physical integrity of the nanowire. If this adhesion is weak, the total length of the nanowire needs to be adjusted so that nanowire segments do not break during different steps of fabrication/suspension.

4. Conclusions

We have demonstrated template directed synthesis of multisegmented nanowires with precise control over segment lengths to ensure functional behavior of each segment. Using a simple, versatile, and cost-effective magnetic assembly technique multisegmented nanowires with conducting polymers as the segment of interest were assembled with precise spatial control. These devices showed semiconducting behavior with high sensitivity towards temperature variations and light exposure. When used as a gas sensor it showed response towards ammonia through charge transfer mechanism. As a part of further investigation we

will fabricate high density nanodevices including sensor arrays and optoelectronic devices using multi-functional nanowires and magnetic assembly. The middle segments can be readily replaced with various electrodeposited metals, metal oxides, semiconductors and conducting polymers depending on applications.

5. Acknowledgements

This material is based on research sponsored by the National Institute of Environmental Health Sciences under agreement number (grant # U01ES016026) and the Defense Microelectronics Activity (DMEA) under agreement number DOD/DMEA-CNN H94003-06-20604 and valuable help from Mrs. Leelaprasanna Vani and Dr. Jianlin Liu from the Electrical Engineering Department, UCR. MAB acknowledges the financial support from UC Graduate Research and Education in Adaptive Bio-Technology Training (GREAT) program. The United States government is authorized to reproduce and distribute reprints for government purposes, not withstanding any copyright notation thereon.

6. References

- [1] A. G. MacDiarmid, *Synth. Met.* **2002**, *125*, 11.
- [2] A. J. Heeger, *Synth. Met.* **2002**, *125*, 23.
- [3] H. Shirakawa, *Synth. Met.* **2002**, *125*, 3.
- [4] L. Dai, P. Soundarrajan, T. Kim, *Pure Appl. Chem.* **2002**, *74*, 1753.
- [5] G. Bidan, *Sens. Actuators B* **1992**, *6*, 45.
- [6] W. Schuhmann, in *Enzyme and Microbial Biosensors: Techniques and Protocols* (Eds: A. Mulchandani, K. R. Rogers), Humana Press, N. J. Totowa, **1998**, pp. 143–156
- [7] K. Ramanathan, M. A. Bangar, M. Yun, W. Chen, N. V. Myung, A. Mulchandani, *J. Am. Chem. Soc.* **2005**, *127*, 496.
- [8] R. M. Hernandez, L. Richter, S. Semanick, S. Stranick, T. E. Mallouk, *Chem. Mater.* **2004**, *16*, 3431.
- [9] A. K. Wanekaya, W. Chen, N. V. Myung, A. Mulchandani, *Electroanalysis* **2006**, *18*, 533.
- [10] K. Ramanathan, S. Annapoorni, B. D. Malhotra, *Sens. Actuators B* **1994**, *21*, 165.
- [11] K. Kim, J. Jin II, *Nano Lett.* **2001**, *11*, 631.
- [12] G. A. O'Brien, A. J. Quinn, D. A. Tanner, G. Redmond, *Adv. Mater.* **2006**, *18*, 2379.
- [13] H. S. White, G. P. Kittlesen, M. S. Wrighton, *J. Am. Chem. Soc.* **1984**, *106*, 5375.
- [14] G. P. Kittlesen, H. S. White, M. S. Wrighton, *J. Am. Chem. Soc.* **1984**, *106*, 7389.
- [15] J. Joo, B. H. Kim, D. H. Park, H. S. Kim, D. S. Seo, J. H. Shim, S. J. Lee, K. S. Ryu, K. Kim, J.-I. Jin, T. J. Lee, C. J. Lee, *Synth. Met.* **2005**, *153*, 313.
- [16] S. Park, S.-W. Chung, C. A. Mirkin, *J. Am. Chem. Soc.* **2004**, *126*, 11772.
- [17] J.-H. Lim, C. A. Mirkin, *Adv. Mater.* **2002**, *14*, 1474.
- [18] B. W. Maynor, S. F. Filocamo, M. W. Grinstaff, J. Liu, *J. Am. Chem. Soc.* **2002**, *124*, 522.
- [19] J. F. Yu, S. Holdcroft, *Chem. Commun.* **2001**, *14*, 1274.
- [20] J. Kameoka, H. G. Craighead, *Appl. Phys. Lett.* **2003**, *83*, 371.
- [21] J. Kameoka, R. Orth, Y. Yang, D. Czaplewski, R. Mathers, G. W. Coates, H. G. Craighead, *Nanotechnology* **2003**, *14*, 1124.
- [22] H. Liu, J. Kameoka, D. A. Czaplewski, H. G. Craighead, *Nano Lett.* **2004**, *4*, 671.
- [23] H. X. He, C. Z. Li, T. J. Tao, *Appl. Phys. Lett.* **2004**, *84*, 828.
- [24] K. Ramanathan, M. A. Bangar, M. H. Yun, W. Chen, A. Mulchandani, N. V. Myung, *Nano Lett.* **2004**, *4*, 1237.
- [25] M. Yun, N. V. Myung, R. P. Vasquez, C. Lee, E. Menke, R. M. Penner, *Nano Lett.* **2004**, *4*, 419.
- [26] E. W. H. Jager, E. Smela, O. Inganas, *Science* **2000**, *290*, 1540.
- [27] H. J. Chung, H. H. Jung, Y. S. Cho, S. Lee, J. H. Ha, J. H. Choi, Y. Kuk, *Appl. Phys. Lett.* **2005**, *86*, art. no. 213113.
- [28] B. H. Kim, D. H. Park, J. Joo, S. G. Yu, S. H. Lee, *Synth. Met.* **2005**, *150*, 279.
- [29] S. C. Hernandez, D. Chaudhuri, W. Chen, N. V. Myung, A. Mulchandani, *Electroanalysis* **2007**, *19*, 2125.
- [30] Q. Ameer, S. B. Adeloju, *Sens. Actuators B* **2005**, *106*, 541.
- [31] S. Mubeen, T. Zhang, B.-Y. Yoo, M. A. Deshusses, N. V. Myung, *J. Phys. Chem. C* **2007**, *111*, 6321.
- [32] T. Zhang, S. Mubeen, E. Bekyarova, B.-Y. Yoo, R. C. Haddon, N. V. Myung, M. A. Deshusses, *Nanotechnology* **2007**, *18*, art. no. 165504.
- [33] R. Ferre, K. Ounadjela, J. M. George, L. Piroux, S. Dubois, *Phys. Rev. B* **1997**, *56*, 14066.
- [34] J. Shen, Z. Chen, N. Wang, H. Yan, G. Shi, A. Jin, C. Gu, *Appl. Phys. Lett.* **2006**, *88*, art. no. 253106.
- [35] J. Joo, K. T. Park, B. H. Kim, M. S. Kim, S. Y. Lee, C. K. Jeong, J. K. Lee, D. H. Park, W. K. Yi, S. H. Lee, K. S. Ryu, *Synth. Met.* **2003**, *135–136*, 7.
- [36] M.-S. Kang, K.-H. Kim, S. Chung, Y. Son, *J. Colloid Interf. Sci.* **2006**, *300*, 259.
- [37] D. Moses, H. Okumoto, D. Comoretto, C. H. Lee, A. J. Heeger, T. Ohnishi, T. Noguchi, *Synth. Met.* **1997**, *84*, 539.
- [38] J. Choi, J. Hormes, P. K. Kahol, *Appl. Phys. Lett.* **2003**, *83*, 2288.
- [39] D. H. Park, B. H. Kim, M. G. Jang, K. Y. Bae, J. Joo, *Appl. Phys. Lett.* **2005**, *86*, art. no. 113116.